Supporting Information for

Generation of Anisotropic Massless Dirac Fermions and Asymmetric Klein Tunneling in Few-Layer Black Phosphorus Superlattices

Zhenglu Li, Ting Cao, Meng Wu, and Steven G. Louie*

Department of Physics, University of California at Berkeley, Berkeley, California 94720, USA and Materials Sciences Division, Lawrence Berkeley National Laboratory, Berkeley, California 94720, USA

*E-mail: sglouie@berkeley.edu

I. Three realistic potential profiles and superlattice periodicity dependence

In the main text, our initial discussions are based on a simple form of potential, as defined in eq 3. Here we give details of three realistic cases also considered – a conical potential mimicking the molecular assembly (Figure S1a), a rectangular potential which can be realized with patterned electrostatic gating (Figure S2a), and a harmonic potential (Figure S3a). A potential can in general be written as the superposition of its Fourier components, i.e., $U(\boldsymbol{r}) = \sum_{\boldsymbol{G}} U(\boldsymbol{G}) e^{i\boldsymbol{G}\cdot\boldsymbol{r}}$. Since the potential is inversely designed from eqs 2–5 in the main text, the lowest $\boldsymbol{G}$ components, which defines the size and shape of the superlattice, are similar to those defined in eq 3 in the main text. In the conical potential, a small deviation from eq 3 exists and effectively shifts the positions of the Dirac points away from the $\boldsymbol{K}_j$ points. However, if the profile of the potential is very localized (such as in molecule assembly), the analysis in the main text can still be treated as a good approximation to the realistic situation. Therefore, our conclusions on the generation of massless Dirac fermions around $\boldsymbol{K}_j$ points are valid, despite the fact that the detailed band structure in other regions away from $\boldsymbol{k}$ = 0 may vary depending on the higher $\boldsymbol{G}$ components of the potential. The periodicity of the conical potential is 2.35 nm, which is quite accessible in experiments, e.g., the assembly of monoxide molecules on Cu (111) surface takes a periodicity of less than 2 nm. The periodicity of the rectangular potential is 7.84 nm, in the same order of magnitude of what has been achieved with current lithographic techniques that can usually reach 10 – 20 nm. The periodicity of the harmonic potential is 2.35 nm, and we use it to enrich the discussions.

Figure S1b and c, Figure S2b and c and Figure S3b and c show the band structures from the three types of potentials, respectively. The anisotropic linear dispersions are clearly seen. Note that for all potentials, the density of states (DOS) show the V-shape feature and a vanishing point.

We further discuss the dependence of superlattice periodicity in the electronic structures. As is shown in Figure S4, we consider the sinusoidal potential (eq 3) with different lattice constants. A smaller periodicity gives a wider energy window for the generated massless Dirac fermions, i.e., the range of linearity.

II. Isolation of the new Dirac fermions within an energy window

Applying the external potential shifts and redistributes the DOS, creating an energy windows where only those newly generated anisotropic Dirac fermions exist. Tuning the Fermi level to such an energy window requires a carrier density in the order of 10^{12} – 10^{13} cm^{-2}, which is quite

achievable experimentally. Noticing that the DOS plotted in Figure 2d, Figure S1d, and Figure S2d only contain the effects of the external potential on the original lowest-energy conduction band, whereas in a real material, other bands need to be considered as well, because they may appear in the same energy window where the Dirac fermions exist, and therefore affect the experimental measurements. Previous *ab initio* calculations (Ref. 27 in the main text) show that in a monolayer black phosphorus, there are other bands ~ 0.2 eV higher in energy than the conduction band minimum and ~ 0.5 eV in energy lower than the valence band maximum. When the number of layers increases to four, other conduction band states almost reach the same energy as conduction band minimum, but those in the valence bands are still at ~ 0.5 eV away from the valence band maximum. Considering the energy of the new Dirac points and potentially interfering states, hole doping in few-layer black phosphorus should be more robust in the generation of isolated-in-energy anisotropic Dirac fermions. However, the ratio of the effective masses along two crystal axes in the hole doping regime varies a lot with number of layers (γ_0 is ~ 1/6 in monolayer with hole doping), while it is almost a constant as a function of layer number in conduction bands; therefore, much care is needed in designing the external potential for a sample with a particular number of layers and the choice of electron or hole doping. Nevertheless, our analyses and calculations in the main text and above based on the conduction band states are quite general, and can be easily applied to the valence band and other systems having anisotropic two-dimensional electron gases.

III. Solving for asymmetric Klein tunneling

The crystal axes of few-layer black phosphorus and the superlattices are defined in the *x*-*y* coordinate system, and the potential barrier is defined in the *x'*-*y'* coordinate system. Vectors and angles in the *x'*-*y'* coordinate system are denoted with a prime symbol. We consider group velocity $\boldsymbol{v}$ of the incident wave packet that can hit the potential barrier, so $\phi_{\boldsymbol{v}}' \in \left[-\frac{\pi}{2}, \frac{\pi}{2}\right]$. With a given $\phi_{\boldsymbol{v}}'$ ($\phi_{\boldsymbol{v}} = \phi_{\boldsymbol{v}}' + \alpha$), because $\tan\phi_{\boldsymbol{k}} = \frac{k_y}{k_x}$ and $\tan\phi_{\boldsymbol{v}} = \gamma_0^2 \frac{k_y}{k_x}$, $\phi_{\boldsymbol{k}}$ can be determined (depending on $\lambda = \pm 1$), and we can write the incident wavevector in region I as $\boldsymbol{k} = (k_x, k_y) = (|k|\cos\phi_{\boldsymbol{k}}, |k|\sin\phi_{\boldsymbol{k}})$, satisfying

$$E_0 = \lambda\frac{\hbar}{2}v_0\sqrt{k_x^2 + \gamma_0^2 k_y^2} = \lambda\frac{\hbar}{2}v_0\sqrt{k^2(\cos^2\phi_{\boldsymbol{k}} + \gamma_0^2\sin^2\phi_{\boldsymbol{k}})}, \tag{S1}$$

and we then have

$$|k| = \frac{2|E_0|}{\hbar v_0}(\cos^2\phi_{\boldsymbol{k}} + \gamma_0^2\sin^2\phi_{\boldsymbol{k}})^{-\frac{1}{2}}, \tag{S2}$$

The same vector is represented in the *x'*-*y'* coordinate system as $\boldsymbol{k} = (|k|\cos\phi_{\boldsymbol{k}}', |k|\sin\phi_{\boldsymbol{k}}')$ where $\phi_{\boldsymbol{k}}' = \phi_{\boldsymbol{k}} - \alpha$. In region I, the reflected wavevector takes $\boldsymbol{k}^r = (k_{x'}^r, k_{y'})$ in the *x'*-*y'* coordinate system, because of $k_{y'}$ conservation. In the *x*-*y* coordinate system, the reflected wavevector reads

$$\begin{aligned} k_x^r &= k_{x'}^r\cos\alpha - k_{y'}\sin\alpha, \\ k_y^r &= k_{x'}^r\sin\alpha + k_{y'}\cos\alpha, \end{aligned} \tag{S3}$$

satisfying

$$k_x^{r2} + \gamma_0^2 k_y^{r2} = \frac{4E_0^2}{\hbar^2 v_0^2}\ , \tag{S4}$$

and we get the solution of $k_{x'}^r$, as well as the spinor angle $\phi_{\boldsymbol{s}}^r$. In region III, there is only one

wavevector which is the same as $\boldsymbol{k}$.

In region II, the wavevectors are denoted as $\boldsymbol{q}$, $\boldsymbol{q}^r$, with $q_{y'} = q_{y'}^r = k_{y'}$, satisfying

$$E_0 = \lambda' \frac{\hbar}{2} v_0 \sqrt{q_x^2 + \gamma_0^2 q_y^2} + V_0. \tag{S5}$$

where

$$\begin{aligned} q_x &= q_{x'} \cos\alpha - k_{y'} \sin\alpha, \\ q_y &= q_{x'} \sin\alpha + k_{y'} \cos\alpha, \end{aligned} \tag{S6}$$

and equivalently, by solving

$$q_x^2 + \gamma_0^2 q_y^2 = \frac{4(V_0 - E_0)^2}{\hbar^2 v_0^2}, \tag{S7}$$

we can have two solutions for $q_{x'}$, one for incident and the other for reflected wave in region II, depending on the group velocities they associated with. Therefore we obtain the spinor angles $\theta_{\boldsymbol{s}}$ and $\theta_{\boldsymbol{s}}^r$. Note that eqs 6 and 7 in the main text should be combined (*i.e.* considering $\lambda(\lambda') = \pm 1$) to determine which quadrant the wavevector and the group velocity lies in, and the spinor direction is determined by spinor angle and λ (λ') together. In a word, to obtain the solutions, the defining equations of the three vectors should be used, coming from eq 6 in the main text.

In a general asymmetric Klein tunneling process, the normal incidence direction is different from the perfect transmission direction, and this difference can be maximized with given m_x^* and m_y^*. The perfect transmission case corresponds to $\boldsymbol{k} = (k\cos\alpha, k\sin\alpha)$, according to the main text. In this case, if we limit $0 < \alpha < \frac{\pi}{2}$, we can maximize $(\alpha - \phi_{\boldsymbol{v}})$, or equivalently $\tan(\alpha - \phi_{\boldsymbol{v}})$. Together with eq 7 in the main text, we may solve for the maximum value (at $\alpha = \alpha_m$) of the following function

$$\tan(\alpha - \phi_{\boldsymbol{v}}) = \frac{\tan\alpha - \tan\phi_{\boldsymbol{v}}}{1 + \tan\alpha\tan\phi_{\boldsymbol{v}}} = \frac{(1 - \gamma_0^2)\tan\alpha}{1 + \gamma_0^2 \tan^2\alpha}. \tag{S8}$$

Finally, we have

$$\tan\alpha_m = \frac{1}{\gamma_0}. \tag{S9}$$

The maximum $(\alpha - \phi_{\boldsymbol{v}})$ corresponds to $\tan\phi_{\boldsymbol{v},m} = \gamma_0$, and meanwhile $\tan\phi_{\boldsymbol{s},m} = 1$. Therefore, $\phi'_{\boldsymbol{v},m} = \phi_{\boldsymbol{s},m} - \alpha = \arctan\gamma_0 - \arctan\frac{1}{\gamma_0}$.

With the alignment of the potential barrier and the solutions in the three regions determined, starting from eq 8, we can have the following set of equations from the boundary conditions,

$$\begin{cases} 1 + r = a + b, \\ \lambda e^{i\phi_s} + \lambda r e^{i\phi_s^r} = \lambda' a e^{i\theta_s} + \lambda' b e^{i\theta_s^r}, \\ a e^{iq_{x'}D} + b e^{iq_{x'}^r D} = t e^{ik_{x'}D}, \\ \lambda' a e^{i\theta_s + iq_{x'}D} + \lambda' b e^{i\theta_s^r + iq_{x'}^r D} = \lambda t e^{i\phi_s + ik_{x'}D}. \end{cases} \tag{S10}$$

With some algebra, eqs 9 and 10 in the main text can be reached.

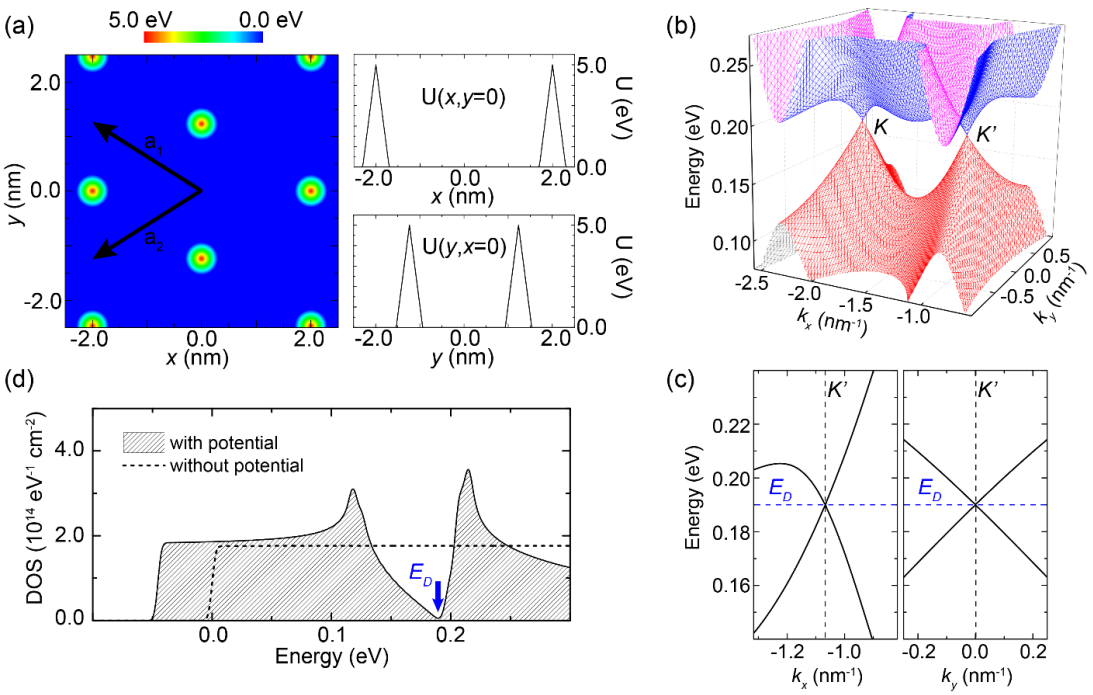

Figure S1. Generation of massless Dirac fermions from a superlattice of conical potentials mimicking the molecule assembly. (a) Real-space distribution of the conical potential of radius 0.3 nm with 2.35 nm periodicity (left panel), along with two line profiles plotted (right two panels). (b) Band structures corresponding to the superlattice potential in (a). (c) Band structures along two normal directions passing through one Dirac point. (d) Density of states (DOS) showing V-shape feature with a vanishing point, with the real electron spin degree of freedom included.

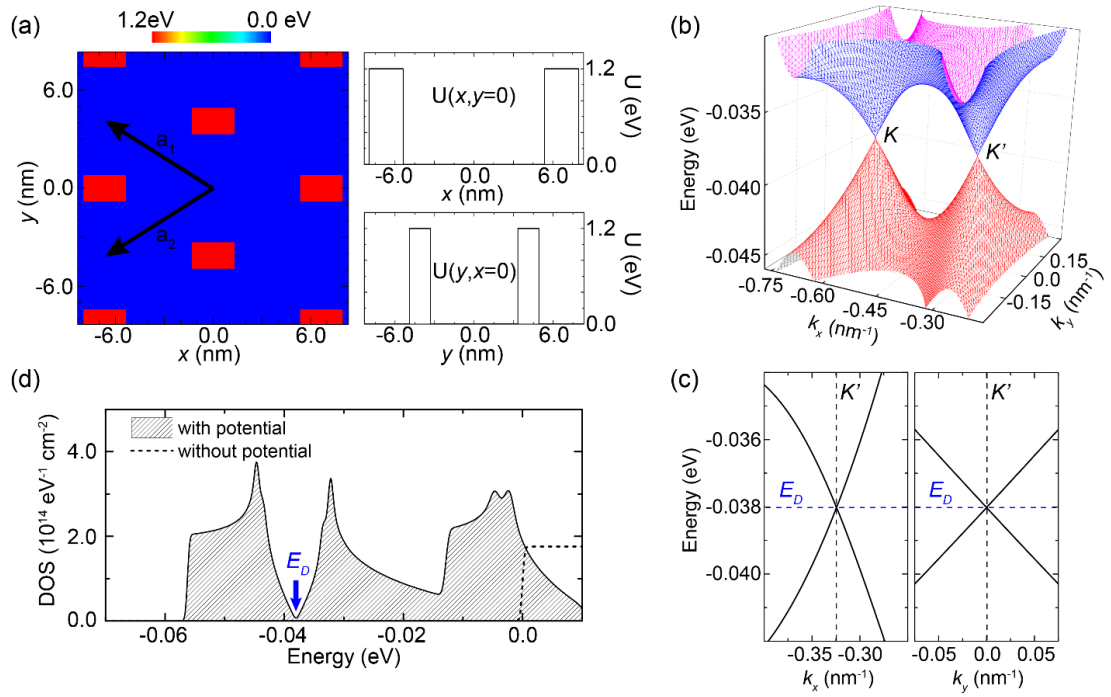

Figure S2. Generation of massless Dirac fermions from a superlattice of rectangular potentials mimicking the patterned electrostatic gating. (a) Real-space distribution of a rectangular potential of 2.67 nm long and 1.65 nm wide with 7.84 nm periodicity (left panel), along with two line profiles plotted (right two panels). (b) Band structures corresponding to the superlattice potential in (a). (c) Band structures along two normal directions passing through one Dirac point. (d) Density of states (DOS) showing V-shape feature with a vanishing point, with the real electron spin degree of freedom included.

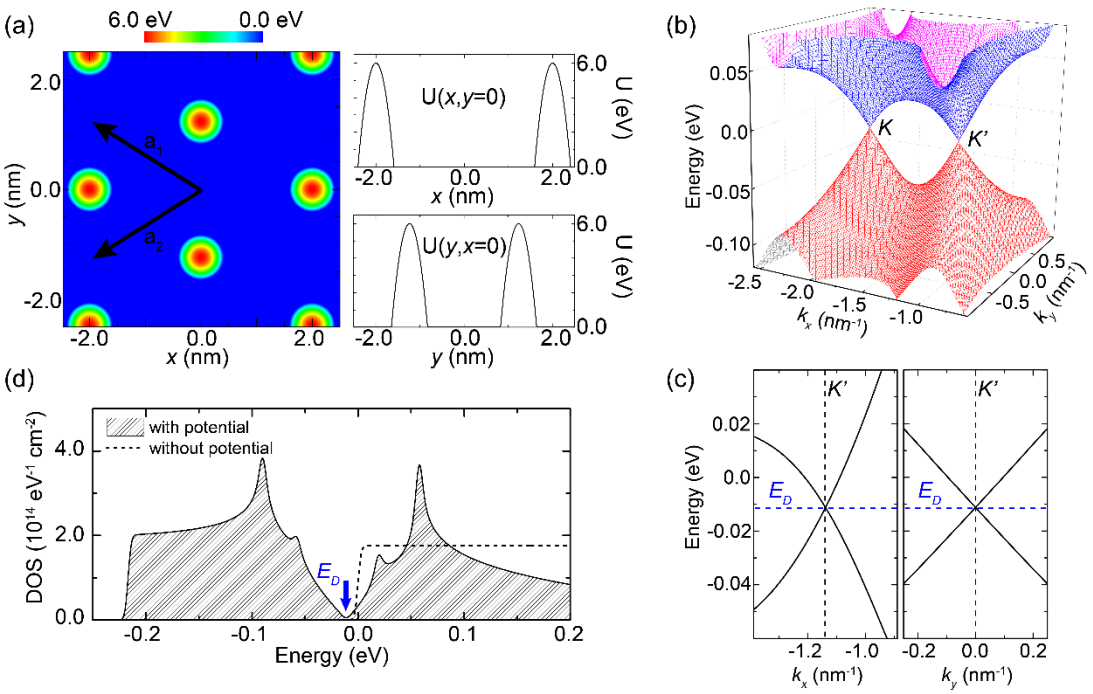

Figure S3. Generation of massless Dirac fermions from a superlattice of harmonic potentials. (a) Real-space distribution of a harmonic potential of radius 0.4 nm with 2.35 nm periodicity (left panel), along with two line profiles plotted (right two panels). (b) Band structures corresponding to the superlattice potential in (a). (c) Band structures along two normal directions passing through one Dirac point. (d) Density of states (DOS) showing V-shape feature with a vanishing point, with the real electron spin degree of freedom included.

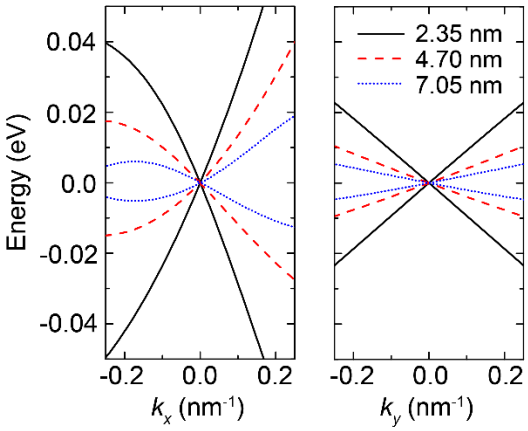

Figure S4. Superlattice periodicity dependence of the electronic band structure of the generated massless Dirac fermions. Three lattice constants are considered; smaller periodicity gives a wider energy window hosting the linearly dispersed Dirac states. Note that in this figure, the k-space and energy origin have been set to the ***K'*** point and the Dirac point energy, respectively, for a direct comparison of the dispersion.